Electrochemical Nucleation of Stable N2 Nanobubbles at Pt Nanoelectrodes

ARTICLE *in* JOURNAL OF THE AMERICAN CHEMICAL SOCIETY · AUGUST 2015

Impact Factor: 12.11 · DOI: 10.1021/jacs.5b07147 · Source: PubMed

JACS
JOURNAL OF THE AMERICAN CHEMICAL SOCIETY

Article

pubs.acs.org/JACS

Electrochemical Nucleation of Stable N_2 Nanobubbles at Pt Nanoelectrodes

Qianjin Chen,[†] Hilke S. Wiedenroth,[†,‡] Sean R. German,[†,§] and Henry S. White*[,†]

[†]Department of Chemistry, University of Utah, 315 S 1400 E, Salt Lake City, Utah 84112, United States

[‡]Department of Environmental and Sustainable Chemistry, Braunschweig University of Technology, Hagenring 30, Braunschweig 38106, Germany

[§]Revalesio Corporation, 1200 East D Street, Tacoma, Washington 98421, United States

Supporting Information

ABSTRACT: Exploring the nucleation of gas bubbles at interfaces is of fundamental interest. Herein, we report the nucleation of individual N_2 nanobubbles at Pt nanodisk electrodes (6−90 nm) via the irreversible electrooxidation of hydrazine ($N_2H_4 \rightarrow N_2 + 4H^+ + 4e^-$). The nucleation and growth of a stable N_2 nanobubble at the Pt electrode is indicated by a sudden drop in voltammetric current, a consequence of restricted mass transport of N_2H_4 to the electrode surface following the liquid-to-gas phase transition. The critical surface concentration of dissolved N_2 required for nanobubble nucleation, $C^s_{N_2,critical}$, obtained from the faradaic current at the moment just prior to bubble formation, is measured to be ∼0.11 M and is independent of the electrode radius and the bulk N_2H_4 concentration. Our results suggest that the size of stable gas bubble nuclei depends only on the local concentration of N_2 near the electrode surface, consistent with previously reported studies of the electrogeneration of H_2 nanobubbles. $C^s_{N_2,critical}$ is ∼160 times larger than the N_2 saturation concentration at room temperature and atmospheric pressure. The residual current for N_2H_4 oxidation after formation of a stable N_2 nanobubble at the electrode surface is proportional to the N_2H_4 concentration as well as the nanoelectrode radius, indicating that the dynamic equilibrium required for the existence of a stable N_2 nanobubble is determined by N_2H_4 electrooxidation at the three phase contact line.

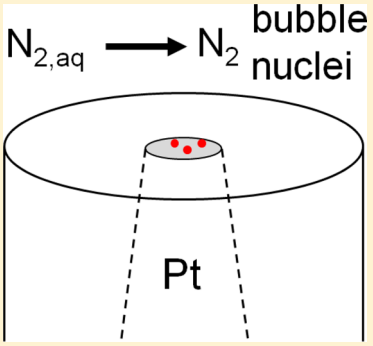

INTRODUCTION

Gas bubbles at solid interfaces are an important research area in surface chemistry, physics, nanofluidics, and chemical engineering. Investigations focus on unraveling the mystery behind bubble nucleation,[1−8] quantifying bubble dynamics as a function of different parameters,[9−11] as well as developing potential applications of nanobubbles in lubrication,[12] cleaning,[13] and synthesizing highly porous metallic surfaces.[14] It has been proposed that interfacial nanobubbles result from a supersaturation of gas at the solid/liquid interface,[1,2] which can be realized by solvent exchange,[9,10] substrate heating,[11,15] or solution decompression.[5−7] Supersaturated solutions are not at equilibrium due to the energy barrier required to form a gas bubble. Upon nucleation, energy is released when dissolved gas molecules at a high chemical potential nucleate a gas phase at a lower partial potential, while formation of a bubble requires additional energy to maintain the surface.[3] In practice, there is a large discrepancy between classical homogeneous nucleation theories and experimental results.[4] For example, theories predict that the threshold concentration of gas needed to cause nucleation should be essentially independent of the gas species used, while experiments demonstrate the opposite.[5−7]

Existence of interfacial nanobubbles and their physical properties is supported by studies using atomic force microscopy in tapping mode (TM-AFM).[8−10,16,17] Several mechanisms have been proposed to explain the long lifetime of surface nanobubbles, including the role of impurities on the bubble surface,[18] dynamic equilibrium,[19] and contact line pinning,[20,21] but still no general agreement has been reached. Recently, electrochemical experiments have advanced fundamental studies of gas nanobubbles, since high overpotentials will readily lead to supersaturation of the solution near the electrode with electrogenerated gas, resulting in heterogeneous nucleation. Bubbles of hydrogen or oxygen from water electrolysis at a gas-evolving electrode were first imaged by photography[22−24] and now by AFM with nanoscopic resolution.[16,17,25] Instead of generating a large ensemble of bubbles on a macroscopic electrode surface, a single nanobubble can also be generated on small electrode surfaces. Recently, we reported the electrogeneration of individual H_2 nanobubbles at Pt nanodisk electrodes with radii <50 nm via the reduction of protons.[26−28] We find that H_2 nanobubble nucleation at the Pt disk electrode occurs at a constant H_2 supersaturation concentration, independent of the electrode size and proton source. These nanobubbles are stabilized by a dynamic equilibrium between the H_2 diffusive outflux and the electrogeneration of H_2 at the three-phase boundary.

Received: July 9, 2015

DOI: 10.1021/jacs.5b07147
J. Am. Chem. Soc. XXXX, XXX, XXX−XXX

Herein, we focus on the electrochemical generation of N_2 nanobubbles from electrooxidation of hydrazine (N_2H_4) on Pt disk nanoelectrodes. N_2H_4 oxidation is of importance in the fields of electroanalysis and electrocatalysis, and the mechanism and kinetics of N_2H_4 oxidation on Pt electrodes have received renewed attention recently.[29−32] In single-particle collision experiments, an electrocatalytic current arises when a single Pt nanoparticle collides with the relatively inactive Au,[33,34] Ni,[35] boron-doped diamond,[36] or carbon-fiber[37] electrode to electrocatalyze N_2H_4 oxidation. The observed "blip" response of the current at a high overpotential is attributed to the deactivation of the Pt nanoparticles, although the possibility of N_2 nanobubble formation has been recently suggested.[35] In the current article, we use Pt disk nanoelectrodes (<90 nm radius) to study N_2H_4 electrooxidation and demonstrate that single nanobubbles of N_2 indeed can be electrochemically generated at the Pt nanoelectrodes (Scheme 1). We further measure the

Scheme 1. Schematic Drawing of the Electrochemical Formation of a Single N_2 Bubble from N_2H_4 Electrooxidation at a Pt Nanodisk Electrode with a Radius of a < ~90 nm

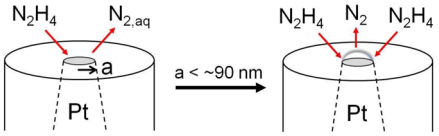

critical concentration of the dissolved gas required for nanobubble nucleation, ~0.11 M, corresponding to a value that is ~160 times larger than the corresponding N_2 saturation concentration at room temperature and atmospheric pressure. The results for N_2 nanobubble nucleation and stability are qualitatively analogous to that for H_2 nanobubble from proton reduction in sulfuric acid solution.[26,27]

EXPERIMENTAL SECTION

Sulfuric acid (Mallinckrodt, 96.2%, ACS grade) and N_2H_4 (Aldrich, 35 wt % in water stored under N_2) were used as received. All aqueous solutions were prepared from deionized water (18.2 MΩ·cm) and were bubbled with N_2 gas to remove dissolved O_2. As shown below, the saturation concentration of dissolved N_2 in the solution at room temperature and ambient pressure (~0.69 mM), resulting from bubbling, is ~0.6% of the concentration required for bubble nucleation. N_2H_4 solutions were freshly prepared daily to reduce the effect of autodecomposition.[38]

Pt nanodisk electrodes were fabricated according to previously reported procedures from our laboratory.[39] Details can be found in the literature as well as our previous reports.[26,28] In order to prepare circular nanodisk electrodes, the electrochemically sharpen Pt wires were carefully aligned along the glass capillaries and then sealed within the glass in H_2 flame.[39] The radii of the nanodisk electrodes, a, were determined from the voltammetric steady-state diffusion-limited current, i_{lim}, for the oxidation of ferrocene ($Fc \rightarrow Fc^+ + e^-$) dissolved in acetonitrile (CH_3CN) containing 0.10 M tetrabutylammonium hexafluorophosphate ($TBAPF_6$). The radii were calculated using the equation:[40,41]

$$i_{lim} = 4nFD_{Fc}C^*_{Fc}a \quad (1)$$

where D_{Fc} (2.4×10^{-5} cm^2/s)[42] and C^*_{Fc} (3.25 mM) are the diffusion coefficient and the bulk concentration of Fc, respectively, and n is the number of electrons transferred per molecule (= 1 for Fc oxidation). Experimental steady-state voltammograms for measuring the electrode radii are presented in Figure S1 in the Supporting Information.

A Dagan Cornerstone Chem-Clamp potentiostat and a Pine RDE4 (used as waveform generator) were interfaced to a computer through a PCI data acquisition card (National Instruments) to collect $i-V$ data. A Ag/AgCl (in 3 M NaCl) electrode and a saturated calomel electrode (SCE) were used as the counter/reference electrode in a two-electrode cell configuration.

RESULTS AND DISCUSSION

Single N_2 nanobubble formation is observed at Pt nanodisk electrodes of radius <90 nm during the oxidation of N_2H_4 when the bulk concentration of N_2H_4 is ≥0.30 M. Figure 1a shows a

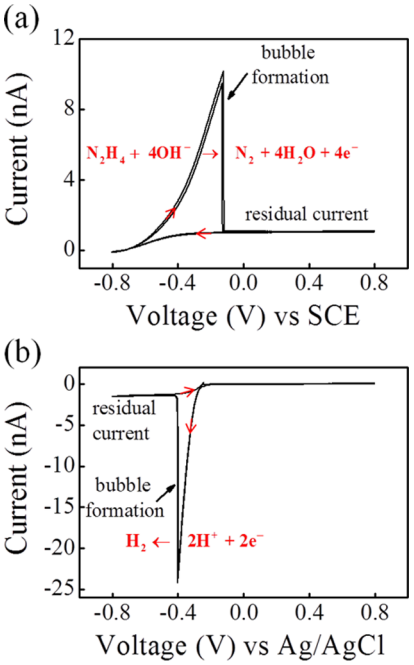

Figure 1. $i-V$ responses of a 32 nm-radius Pt nanoelectrode immersed in (a) 1.0 M N_2H_4 and (b) 0.5 M H_2SO_4 at a scan rate of 200 mV/s. The voltammograms shown are for two scan cycles. The initial potential is −0.80 V in (a) and 0.0 V in (b), respectively, and the arrows indicate the direction of potential scanning.

typical cyclic voltammogram recorded at a 32 nm radius Pt nanodisk electrode immersed into a 1.0 M N_2H_4 solution. At potentials positive of ~−0.70 V versus SCE, close to the thermodynamic potential for N_2H_4 electrooxidation reaction at Pt electrodes,[43] the current associated with N_2H_4 oxidation slowly rises, and the voltammetric shape is controlled by N_2H_4 transport, ohmic loss, as well as the electron-transfer kinetics. The current increases until reaching a peak value, i^p_{nb}, of ~10 nA, and then suddenly drops to a stable residual current of ~1.0 nA. We ascribed this peak-shaped characteristic waveshape to the formation of a single gas nanobubble at the electrode surface. For comparison, the voltammetric response corresponding to single H_2 bubble formation, using the same electrode immersed into a 0.5 M H_2SO_4 solution, is shown in Figure 1b. Note that the voltammetric wave for N_2 bubble formation is drawn out in comparison to H_2 bubble, presumably because of slower electron-transfer kinetics.

After formation of the N_2 nanobubble, the current decreases to a small residual value, i^r_{nb}, which is very stable at potentials positive of the peak potential. The small i^r_{nb} value suggests that the gas nanobubble blocks most of the active Pt surface, reducing the rate of N_2H_4 oxidation. We believe that i^r_{nb}

DOI: 10.1021/jacs.5b07147
J. Am. Chem. Soc. XXXX, XXX, XXX−XXX

corresponds to the rate of N_2 electrogeneration at the electrode surface required to balance the N_2 diffusive outflux from the bubble into the solution. Understanding the factors that control i^r_{nb} provides insight into the mechanism by which a nanobubble remains stable.

Surprisingly, i^P_{nb} for N_2 bubbles is found to depend on the time that the Pt disk electrode is immersed into the N_2H_4 solution. As typified for a 32 nm radius Pt disk electrode, the initial i^P_{nb} from voltammetric responses after a freshly prepared Pt electrode is immersed into the N_2H_4 solution is ~10 nA. As the immersion time increases while continuously scanning the electrode potential, i^P_{nb} decreases gradually and levels off to ~7 nA after 10 min. Control experiments with the electrode disconnected from the cell circuit during the time intervals between two consecutive voltammetric measurements were also conducted, and a very similar decrease in i^P_{nb} was observed, indicating that potential scanning is not required to observe the current decrease. From the literature, the decrease of i^P_{nb} with immersion time is likely due to the known adsorption of N_2H_4 and reaction intermediates at the Pt surface,[44,45] which inhibit the oxidation of N_2H_4, and further affects bubble nucleation. The recovery of i^P_{nb} can be achieved by careful rinsing the electrode with copious amounts of CH_3CN and water (see Supporting Information Figure S2), indicating weak adsorption of adsorbates. Figure 2 shows that the voltammetric response,

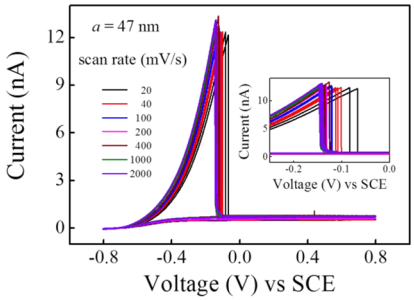

Figure 2. Cyclic voltammograms at different scan rates for a 47 nm-radius disk electrode in 1.0 M N_2H_4 solution obtained at immersion times between 10 and 20 min. Little dependence of i^P_{nb} on the scan rate from 20 mV/s to 2.0 V/s is observed.

including the value of i^P_{nb}, is essentially independent of the scan rate between 20 mV/s to 2 V/s, indicating that the N_2 concentration profile around the electrode surface reaches a steady state within this range of voltammetric scan rates. In quantifying the threshold gas concentration for N_2 bubble nucleation, the initial value of i^P_{nb} for a pristine Pt electrode is believed to more accurately describe the nucleation supersaturation concentration. Thus, throughout the remainder of this paper, i^P_{nb} refers to the initial value obtained from averaging the peak current from voltammetric responses within the first five scan cycles after freshly rinsed electrodes are immersed into the N_2H_4 solution.

Similar to previous results reported for H_2 nanobubble formation, the appearance of a sharp peak in the voltammetric response occurs only at N_2H_4 concentrations above a critical value. Below this value, the voltammetic response of the nanodisk electrode displays a sigmoidal shape that is characteristic of a diffusion-limited response without interference of a liquid-to-gas phase transition. Figure 3a shows voltammograms recorded at a 27 nm radius Pt nanodisk in N_2H_4 solutions below the critical concentration (0.02, 0.05, 0.10, and 0.20 M)

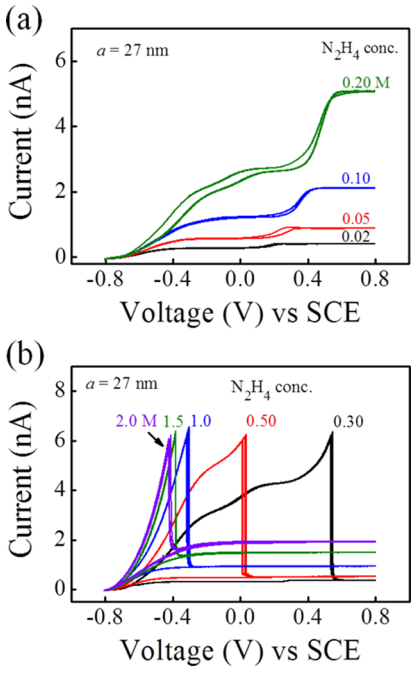

Figure 3. $i-V$ responses of a 27 nm radius Pt nanoelectrode immersed in (a) 0.02, 0.05, 0.10, and 0.20 M N_2H_4, where only sigmodial-shaped waves are observed, and (b) 0.30, 0.50, 1.0, 1.5, and 2.0 M N_2H_4, where peak-shaped waves are observed, at a scan rate of 100 mV/s.

for bubble formation. Unlike the one step sigmoidal shape voltammetric response for proton reduction, the voltammograms for N_2H_4 oxidation in the absence of bubble formation display two current plateaus in solutions containing 0.02, 0.05, and 0.10 M N_2H_4 (and likely three current plateaus for 0.20 M N_2H_4), indicating that the N_2H_4 oxidation reaction at Pt nanoelectrodes is a multiple-step reaction with several redox-active intermediates. We find that the limiting current for both the plateau between 0.1 and 0.2 V and the plateau at 0.8 V increases approximately linearly with the N_2H_4 concentration. From previous studies, it was concluded that N_2H_4 electrooxidation at Pt electrodes takes place as a stepwise electrochemical dehydrogenation process with dissolved N_2 as the main product.[46,47] Different step reaction mechanisms and intermediates have been proposed, which vary both as a function of the nature and structure of the electrode surface and electrolyte composition/pH.[30,48]

$$N_2H_5^+ \rightarrow N_2 + 5H^+ + 4e^- \quad \text{(low pH)} \tag{2}$$

$$N_2H_4 + 4OH^- \rightarrow N_2 + 4H_2O + 4e^- \quad \text{(high pH)} \tag{3}$$

Further discussion of hydrazine electrooxdation mechanism at Pt electrodes is beyond the scope of this paper and can be found in a comprehensive review elsewhere.[48] Given that the overall number of electrons transferred per N_2H_4 molecule is 4, we obtain a diffusivity of 6.1×10^{-6} cm^2/s from the limiting current of 5.07 nA at the 27 nm disk electrode in a 0.20 M N_2H_4 solution ($i_{lim} = 4nFDCa$), which lies within the range of reported values ($0.5-1.5 \times 10^{-5}$ cm^2/s).[36,46,49,50]

Despite the complexity of the mechanism of N_2H_4 oxidation, the key finding is that peak-shaped voltammetric responses are consistently observed in solutions containing a concentration of 0.30 M or greater, as demonstrated in Figure 3b. Remarkably, the N_2 nanobubble peak current i^P_{nb} at the 27 nm radius disk electrode remains constant at ~6 nA as the N_2H_4 concentration

DOI: 10.1021/jacs.5b07147
J. Am. Chem. Soc. XXXX, XXX, XXX−XXX

further increases, indicating that the bubble nucleation is determined by a critical N_2 concentration at the electrode surface, rather than the concentration of N_2H_4 available for oxidation. The multiple current plateaus before bubble formation for 0.30 and 0.50 M N_2H_4 solutions, Figure 3, further suggest the stepwise N_2H_4 electrooxidation reaction. The nanobubble peak potential shifts from 0.54 V for 0.30 M N_2H_4 to a much lower potential of −0.42 V for 2.0 M N_2H_4. The drawn out cyclic voltammogram at low N_2H_4 concentration is analogous to that observed for the H_2 bubble nucleation in a weak acid solution, e.g., acetic acid, as previously reported.[26,27] Additional overpotential drives the pre-equilibrium dissociation of the weak acid prior to proton reduction to allow sufficient H_2 electrogeneration to nucleate a gas nanobubble. The large shift in the nanobubble peak potential with N_2H_4 concentration suggests that N_2H_4 electrooxidation is limited by electron-transfer kinetics, rather than mass transport. In summary, at low N_2H_4 concentrations, the corresponding concentration of electrogenerated N_2 at the electrode surface fails to achieve the value required for bubble nucleation, while at higher N_2H_4 concentrations, the concentration of N_2 molecules is sufficient to nucleate a nanobubble; this critical N_2 concentration is independent of the bulk concentration of N_2H_4.

Since nanobubbles at interfaces are extremely sensitive to surfactants or contaminants,[18] ultrapure water was used as the electrolyte, and subsequently a significant ohmic drop occurs between the electrodes. To confirm that our results are not overly distorted by the solution resistance, a 1.0 M N_2H_4 solution containing 0.20 M KCl as supporting electrolyte was also investigated. As shown in Figure 4, the cyclic voltammogram in the presence of 0.20 M KCl rises more steeply than without KCl, indicating that the drawn out wave in the absence of supporting electrolyte is partly due to the resistive drop between the electrodes. However, regardless of whether or not the solution contains a supporting electrolyte, the peak current corresponding to bubble formation remains constant, further confirming our hypothesis that a constant critical gas concentration for nucleation.

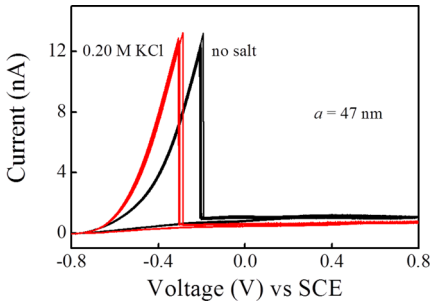

Figure 4. Cyclic voltammograms at 200 mV/s for a 47 nm radius disk electrode in 1.0 M N_2H_4 with (red line) and without (black line) 0.20 M KCl as supporting electrolyte.

The residual current after bubble formation is also approximately the same after salt addition, consistent with previous electrochemical studies on H_2 bubble formation, where no change of residual current was observed when inert salts (KCl, Na_2SO_4, sodium citrate) were added to the 0.5 M H_2SO_4 solution.[27] Studies of the effects of salts on the interfacial nanobubble stability using TM-AFM also concluded that surface nanobubbles, once formed, were insensitive to the addition of salts.[10]

We now consider the effect of Pt electrode radii on bubble nucleation. In the case of proton reduction, a peak shape voltammetric response corresponding to the H_2 bubble formation is consistently observed only for nanodisks with radii <~50 nm, whereas for radii >~50 nm, a sigmoidal-shaped voltammetry with significant hysteresis is observed. The maximum Pt electrode radius to reproducibly form a N_2 nanobubble is found to be ~90 nm. Figure 5 shows typical cyclic voltammograms recorded at Pt nanodisk electrodes of different radii immersed in 1.0 M N_2H_4 solution. For a 5.8 nm radius electrode, the peak current i_{nb}^{P} at which a N_2 nanobubble nucleates is ~3.1 nA, while for a 54 nm radius electrode, i_{nb}^{P} increases to ~17.8 nA. In contrast, for an electrode above the 90 nm critical radius, the cyclic voltammetric response displays a sigmoidal-shape with large hysteresis between the forward and backward scan (see Supporting Information Figure S3). Why dissolved N_2 molecules do not nucleate into a bubble to cover the entire electrode surface for $a > \sim 90$ nm is not understood.

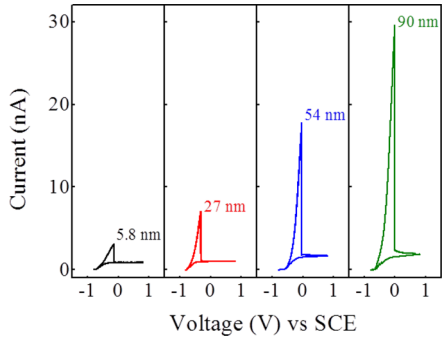

Figure 5. $i-V$ responses of Pt nanoelectrodes with radii of 5.8, 27, 54, and 90 nm in 1.0 M N_2H_4 at a scan rate of 200 mV/s.

Assuming that the voltammetric current exclusively arises from the N_2 electrogeneration and the system is at steady state prior to the liquid-to-gas transition, the measured current can be correlated to the diffusion of N_2 away from the electrode surface using the expression:

$$i_{nb}^{P} = 4nFD_{N_2}C_{N_2,critical}^{s}a \quad (4)$$

where D_{N_2} is the diffusivity of N_2 (1.9×10^{-5} cm^2/s),[51] and n is the number of electrons transferred per formation of a gas molecule (= 4 for N_2). Eq 4 relates the N_2 surface concentration, $C_{N_2,critical}^{s}$, to the peak current, i_{nb}^{P}, at the moment just prior to bubble nucleation. Eq 4 assumes diffusion of N_2 away from the disk shape electrode surface and is derived from Fick's laws.[40,41] Based on the independent measurements using different disk nanoelectrodes, we find that i_{nb}^{P} is proportional to electrode radii, as shown in Figure 6. The slope from the linear plot of i_{nb}^{P} vs a yields the critical surface concentration $C_{N_2,critical}^{s}$ of 0.11 ± 0.01 M for N_2, corresponding to an ~160-fold increase above the saturation value at room temperature and atmospheric pressure (~0.69 mM). Interestingly, such a supersaturation value (~160) required to cause N_2 bubble nucleation agrees well with the range of 180−190 reported by Hemmingsen[5−7] and 136 by Finkelstein and Tamir[52] using the classical cavitation method, where the aqueous solutions are equilibrated with N_2 at a high pressure and then suddenly

DOI: 10.1021/jacs.5b07147
J. Am. Chem. Soc. XXXX, XXX, XXX−XXX

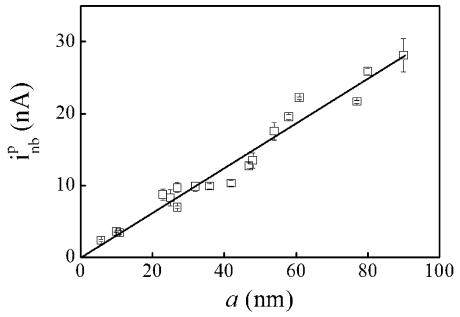

Figure 6. N_2 nanobubble peak current, i^{p}_{nb}, as a function of nanoelectrode radii for N_2 bubble nucleation in 1.0 M N_2H_4.

decompressed to observe gas bubbles. These threshold supersaturation concentrations were found for bubbles at the glass/water interface, hence heterogeneous bubble nucleation was likely being observed. On the other hand, N_2 gas supersaturation can also be achieved by the fast decomposition of aqueous nitrite.[53,54] The threshold concentration for homogeneous nucleation in aqueous solution was reported to be 23−100 times the N_2 solubility at 1 atm, depending on the solution ionic strength. However, it is generally accepted that heterogeneous nucleation is substantially faster than homogeneous nucleation due to the pronounced decrease of the critical nucleation energy barrier; this common belief is inconsistent with the above experimentally reported nucleation supersaturation value for N_2 bubble nucleation.

Once formed, we speculate that the stability of a nanobubble should result from a dynamic equilibrium between the N_2 diffusive outflux through the nanobubble/liquid interface (controlled by Henry's law and gas-molecule transfer kinetics) and further N_2 influx into the bubble from gas electrogeneration at the three phase contact line. A similar dynamic equilibrium mechanism for surface nanobubble stabilization has been previously theoretically considered by Brenner,[19] suggesting that the diffusive outflux of gas is compensated by a continuous influx of gas near the contact line, due to gas attraction toward hydrophobic walls. In our study, the influx of gas required to balance the diffusive outflux for a stable nanobubble at an electrode surface can be experimentally measured from the residual current (see Scheme 2). In the following paragraphs, we discuss the stability of a nanobubble at an electrode surface in terms of the measured residual current.

Scheme 2. Sketch of Gas Outflux and Influx into the Surface Nanobubble

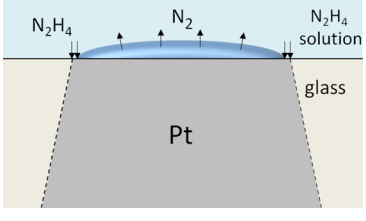

As shown in Figures 1 and 3, after the formation of a nanobubble, the current decreases to a residual current, i^{r}_{nb}. Because of the small size of the Pt disks and the high consistency of the voltammetric results using different electrodes, we believe that the gas nanobubble covers the majority of the surface and that N_2H_4 oxidation associated with the small

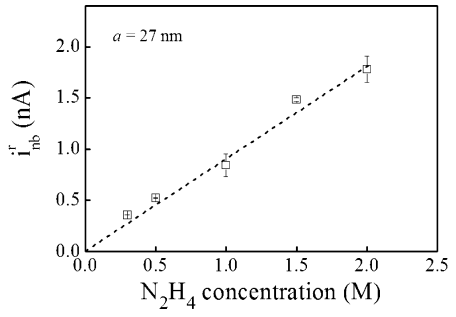

Figure 7. Dependence of the residual current, i^{r}_{nb}, at 0.8 V from voltammetric response at 100 mV/s for a 27 nm radius disk electrode in N_2H_4 aqueous solutions with different concentrations (0.30, 0.50, 1.0, 1.5, 2.0 M) in Figure 3b.

i^{r}_{nb} exclusively occurs at the circumference of the Pt disk electrode. In Figure 3b, i^{r}_{nb} after bubble formation for a given 27 nm radius nanoelectrode is quite stable, essentially independent of the potential. Figure 7 shows that the i^{r}_{nb} obtained in Figure 3b is proportional to the N_2H_4 concentration, suggesting that N_2H_4 transport to the three phase contact line for further gas generation is likely to be the rate-limiting step in establishing the nanobubble dynamic equilibrium. Clearly if N_2 diffusional outflux were rate limiting, i^{r}_{nb} would not scale linearly with the N_2H_4 concentration. Surprisingly, in our previous studies of H_2 nanobubble stability, a linear dependence of i^{r}_{nb} on proton concentration for a given electrode was not observed.[26,27]

Figure 8 further shows, within experimental error, an approximately linear relationship between i^{r}_{nb} at 1.0 M N_2H_4

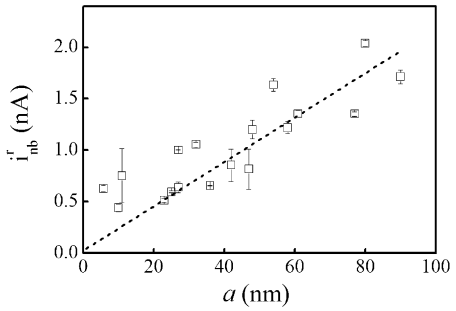

Figure 8. Dependence of the residual current, i^{r}_{nb}, at 0.8 V from voltammetric response at 100 mV/s as a function of nanoelectrode radii at 1.0 M N_2H_4 solution.

and the radii of nanoelectrodes used for N_2 bubble formation, consistent again with the nanobubble dynamic equilibrium being limited by the size of the three phase contact line available for gas electrogeneration. In summary and, as indicated in Scheme 2, we conclude that the dynamic equilibrium for the nanobubble at the electrode surface is limited by N_2 electrogeneration, which is dependent both on the bulk N_2H_4 concentration and the length of active three phase contact line.

CONCLUSIONS

In summary, this study demonstrates that single N_2 nanobubbles can be electrochemically generated from N_2H_4 electrooxidation at Pt nanoelectrodes with radii <~90 nm. The voltammetric current suddenly decreases (~93% blockage) as a gas nanobubble forms at the electrode and blocks N_2H_4 transport to the surface. We find that the peak currents at the

DOI: 10.1021/jacs.5b07147
J. Am. Chem. Soc. XXXX, XXX, XXX−XXX

moment of bubble nucleation are proportional to the Pt nanoelectrode radii, but independent of N_2H_4 concentration. The critical surface concentration for N_2 nanobubble nucleation is measured to be 0.11 ± 0.01 M, corresponding to ~160 times the saturation value at room temperature and atmospheric pressure, consistent with the results of heterogeneous nucleation from classical cavitation methods. After bubble formation, the residual current is proportional to the N_2H_4 concentration as well as the nanoelectrode radii, implying that the nanobubble dynamic equilibrium is limited by the N_2 influx from gas electrogeneration at the three phase contact line. Finally, we suggest that the "blip" current response feature for single Pt nanoparticles collision at a Ni microelectrode, corresponding to the electrocatalytic oxidation of N_2H_4 (reported in ref 35) is unlikely to be due to the N_2 nanobubble formation at the surface of Pt nanoparticle. The N_2H_4 concentration used in that study (8.7 mM) is much lower than the critical concentration required to form a gas nanobubble found in our study (0.30 M).

■ ASSOCIATED CONTENT

Supporting Information

The Supporting Information is available free of charge on the ACS Publications website at DOI: 10.1021/jacs.5b07147.

Characterization of Pt nanodisk electrodes; dependence of voltammetric responses on immersion time; voltammetric response of a 98 nm radius Pt electrode (PDF)

■ AUTHOR INFORMATION

Corresponding Author

*white@chem.utah.edu

Notes

The authors declare no competing financial interest.

■ ACKNOWLEDGMENTS

This work was supported by the Office of Naval Research.

■ REFERENCES

(1) Jones, S. F.; Evans, G. M.; Galvin, K. P. *Adv. Colloid Interface Sci.* **1999**, *80*, 27−50.
(2) Dammer, S. M.; Lohse, D. *Phys. Rev. Lett.* **2006**, *96*, 206101.
(3) Weathersby, P. K. *J. Appl. Physiol.: Respir., Environ. Exercise Physiol.* **1982**, *53*, 940−946.
(4) Lubetkin, S. D. *Langmuir* **2003**, *19*, 2575−2587.
(5) Hemmingsen, E. A. *J. Appl. Phys.* **1975**, *46*, 213−218.
(6) Gerth, W. A.; Hemmingsen, E. A. *Z. Naturforsch., A: Phys. Sci.* **1976**, *31*, 1711−1716.
(7) Hemmingsen, E. A. *Nature* **1977**, *267*, 141−142.
(8) Seddon, J. R. T.; Kooij, E. S.; Poelsema, B.; Zandvliet, H. J. W.; Lohse, D. *Phys. Rev. Lett.* **2011**, *106*, 056101.
(9) Lou, S.-T.; Ouyang, Z.-Q.; Zhang, Y.; Li, X.-J.; Hu, J.; Li, M.-Q.; Yang, F.-J. *J. Vac. Sci. Technol., B: Microelectron. Process. Phenom.* **2000**, *18*, 2573−2575.
(10) Zhang, X. H.; Maeda, N.; Craig, V. S. J. *Langmuir* **2006**, *22*, 5025−5035.
(11) Yang, S.; Dammer, S. M.; Bremond, N.; Zandvliet, H. J. W.; Kooij, E. S.; Lohse, D. *Langmuir* **2007**, *23*, 7072−7077.
(12) Lauga, E.; Brenner, M. *Phys. Rev. E* **2004**, *70*, 026311.
(13) Liu, G.; Wu, Z.; Craig, V. S. J. *J. Phys. Chem. C* **2008**, *112*, 16748−16753.
(14) Plowman, B. J.; Jones, L. A.; Bhargava, S. K. *Chem. Commun.* **2015**, *51*, 4331−4346.
(15) Zhang, X. H.; Zhang, X. D.; Lou, S. T.; Zhang, Z. X.; Sun, J. L.; Hu, J. *Langmuir* **2004**, *20*, 3813−3815.
(16) Zhang, L.; Zhang, Y.; Zhang, X.; Li, Z.; Shen, G.; Ye, M.; Fan, C.; Fang, H.; Hu, J. *Langmuir* **2006**, *22*, 8109−8113.
(17) Yang, S.; Tsai, P.; Kooij, E. S.; Prosperetti, A.; Zandvliet, H. J. W.; Lohse, D. *Langmuir* **2009**, *25*, 1466−1474.
(18) Ducker, W. A. *Langmuir* **2009**, *25*, 8907−8910.
(19) Brenner, M. P.; Lohse, D. *Phys. Rev. Lett.* **2008**, *101*, 214505.
(20) Weijs, J. H.; Lohse, D. *Phys. Rev. Lett.* **2013**, *110*, 054501.
(21) Zhang, X.; Chan, D. Y. C.; Wang, D.; Maeda, N. *Langmuir* **2013**, *29*, 1017−1023.
(22) Westerheide, D. E.; Westwater, J. W. *AIChE J.* **1961**, *7*, 357−362.
(23) Dapkus, K. V.; Sides, P. J. *J. Colloid Interface Sci.* **1986**, *111*, 133−151.
(24) Gabrielli, C.; Huet, F.; Keddam, M. *J. Appl. Electrochem.* **1989**, *19*, 617−629.
(25) Nakabayashi, S.; Shinozaki, R.; Senda, Y.; Yoshikawa, H. Y. *J. Phys.: Condens. Matter* **2013**, *25*, 184008.
(26) Luo, L.; White, H. S. *Langmuir* **2013**, *29*, 11169−11175.
(27) Chen, Q.; Luo, L.; Faraji, H.; Feldberg, S. W.; White, H. S. *J. Phys. Chem. Lett.* **2014**, *5*, 3539−3544.
(28) Chen, Q.; Luo, L.; White, H. S. *Langmuir* **2015**, *31*, 4573−4581.
(29) Rosca, V.; Koper, M. T. M. *Electrochim. Acta* **2008**, *53*, 5199−5205.
(30) Aldous, L.; Compton, R. G. *Phys. Chem. Chem. Phys.* **2011**, *13*, 5279−5287.
(31) Chen, C.-H.; Jacobse, L.; McKelvey, K.; Lai, S. C. S.; Koper, M. T. M.; Unwin, P. R. *Anal. Chem.* **2015**, *87*, 5782−5789.
(32) Sanabria-Chinchilla, J.; Asazawa, K.; Sakamoto, T.; Yamada, K.; Tanaka, H.; Strasser, P. *J. Am. Chem. Soc.* **2011**, *133*, 5425−5431.
(33) Xiao, X.; Fan, F.-R. F.; Zhou, J.; Bard, A. J. *J. Am. Chem. Soc.* **2008**, *130*, 16669−16677.
(34) Kwon, S. J.; Bard, A. J. *J. Am. Chem. Soc.* **2012**, *134*, 10777−10779.
(35) Jung, A. R.; Lee, S.; Joo, J. W.; Shin, C.; Bae, H.; Moon, S. G.; Kwon, S. J. *J. Am. Chem. Soc.* **2015**, *137*, 1762−1765.
(36) Wakerley, D.; Guell, A. G.; Hutton, L. A.; Miller, T. S.; Bard, A. J.; Macpherson, J. V. *Chem. Commun.* **2013**, *49*, 5657−5659.
(37) Guo, Z.; Percival, S. J.; Zhang, B. *J. Am. Chem. Soc.* **2014**, *136*, 8879−8882.
(38) Gilbert, E. C. *J. Am. Chem. Soc.* **1929**, *51*, 2744−2751.
(39) Zhang, B.; Zhang, Y.; White, H. S. *Anal. Chem.* **2004**, *76*, 6229−6238.
(40) Saito, Y. *Rev. Polarogr.* **1968**, *15*, 177−182.
(41) Bard, A. J.; Faulkner, L. R. *Electrochemical Methods: Fundamentals and Applications*; 2nd ed.; John Wiley & Sons: New York, 2001.
(42) Kuwana, T.; Bublitz, D. E.; Hoh, G. *J. Am. Chem. Soc.* **1960**, *82*, 5811−5817.
(43) Maloy, J. T. In *Standard Potentials in Aqueous Solutions*; Bard, A. J., Parsons, R., Jordan, J., Eds.; Dekker: New York, 1985; pp 127.
(44) Nishihara, C.; Raspini, I. A.; Kondoh, H.; Shindo, H.; Kaise, M.; Nozoye, H. *J. Electroanal. Chem.* **1992**, *338*, 299−316.
(45) Gómez, R.; Orts, J. M.; Rodes, A.; Feliu, J. M.; Aldaz, A. *J. Electroanal. Chem.* **1993**, *358*, 287−305.
(46) Karp, S.; Meites, L. *J. Am. Chem. Soc.* **1962**, *84*, 906−912.
(47) Szpak, S.; Stonehart, P.; Katan, T. *Electrochim. Acta* **1965**, *10*, 563−583.
(48) Rosca, V.; Duca, M.; de Groot, M. T.; Koper, M. T. M. *Chem. Rev.* **2009**, *109*, 2209−2244.
(49) Bard, A. J. *Anal. Chem.* **1963**, *35*, 1602−1607.
(50) Kleijn, S. E. F.; Lai, S. C. S.; Miller, T. S.; Yanson, A. I.; Koper, M. T. M.; Unwin, P. R. *J. Am. Chem. Soc.* **2012**, *134*, 18558−18561.
(51) Cussler, E. L. *Diffusion: Mass Transfer in Fluid Systems*; 2nd ed.; Cambridge University Press: New York, 1997.
(52) Finkelstein, Y.; Tamir, A. *AIChE J.* **1985**, *31*, 1409−1419.
(53) Rubin, M. B.; Noyes, R. M.; Smith, K. W. *J. Phys. Chem.* **1987**, *91*, 1618−1622.
(54) Rubin, M. B.; Noyes, R. M. *J. Phys. Chem.* **1992**, *96*, 993−1000.